Advanced Devices & Instrumentation
A SCIENCE PARTNER JOURNAL

RESEARCH ARTICLE

Laser Scanning Microscopy for Tomographic Imaging of Roughness and Point Absorbers in Optical Surfaces

Leif Albers, Malte Hagemann, and Roman Schnabel*

Institut für Quantenphysik & Zentrum für Optische Quantentechnologien, Universität Hamburg, Luruper Chaussee 149, 22761 Hamburg, Germany.

*Address correspondence to: roman.schnabel@physnet.uni-hamburg.de

High-precision laser interferometric instruments require optical surfaces with a close to perfect contour, as well as low scattering and absorption. Especially, point absorbers are problematic because they heat up and locally deform the otherwise flat surface, resulting in correlations between absorption and contour. Here, we present a spiral laser scanning microscopy approach for the reconstruction of the 2 complementary images of an optical surface. The "phase image" is related to the surface profile including roughness. Our experiment achieves a sensitivity of up to (3.1±1.4) fm/$\sqrt{\text{Hz}}$ with a (5.29±0.06)-µm transversal resolution. The "loss image" localizes point absorbers. The 2 images show correlations for some features proving the particular strength of our tomographic approach, which should help further improving optical surfaces or to understand dynamic processes of surface physics.

Citation: Albers L, Hagemann M, Schnabel R. Laser Scanning Microscopy for Tomographic Imaging of Roughness and Point Absorbers in Optical Surfaces. *Adv. Devices Instrum.* 2024;5:Article 0064. https://doi.org/10.34133/adi.0064

Submitted 26 January 2024
Revised 13 July 2024
Accepted 1 August 2024
Published 9 October 2024

Introduction

Ultrahigh precision optics play a substantial role in scientific research and technological advancements, ranging from laser gyroscopes [1,2] and optical atomic clocks [3,4] to the detection of gravitational waves [5–7]. The quality of optical components critically influences the performance of these systems. In particular, the remaining surface roughness of super-polished laser mirrors in interferometric setups is a limiting factor, as it produces disturbances due to backscattered light ("parasitic interferences") [8,9]. A further limitation is absorption, particularly by microscopically small "point absorbers", which leads to thermal distortions over large areas at high optical power [10,11]. Profiling and characterizing these attributes with high sensitivity and resolution and finding their correlations are essential for optimizing optics and instruments.

The most commonly used and commercially available techniques for imaging surface roughness are atomic force microscopy and variations of interference microscopy [12,13]. While atomic force microscopy allows for precise surface topography, offering up to atomic resolution, it is typically limited to a small field of view (FOV) and can be quite time-consuming [12–14]. Furthermore, atomic force microscopy does not provide any direct information on optical absorption at a specific wavelength. Interference microscopy methods allow for fast profiling of larger FOVs since they involve 2-dimensional imaging sensors [15–17]. In principle, interference microscopy is able to measure the surface profile and optically absorbing features simultaneously, but they do not provide the surface profile with laser interferometric sensitivity.

Here, we present a fast spiral laser scanning microscopy technique combined with computational image reconstruction. We demonstrate a diffraction-limited transversal resolution of (5.29 ± 0.06) µm and interferometric sensitivity with respect to the surface profile of (3.1±1.4) fm/$\sqrt{\text{Hz}}$ over an example area of more than 50 mm^2, achieved in just a few minutes. Our method maps an optical component in terms of reflection phase as well as optical loss by scanning a focused probe laser in a spiral path across its surface. The spiral scanning avoids reversal points, which increases efficiency. Our images of the surface of a high-quality laser mirror show interesting correlations between the optical loss and the surface profile.

Methods

Experiment

Our setup was based on a Mach–Zehnder interferometer, as illustrated in Fig. 1. We used a 0.5-mW continuous-wave monochromatic laser beam in the TEM_{00} mode with a center wavelength of 1,550 nm, supplied by an NKT Basik Laser module. It was split at a balanced beam splitter (BS1) into a signal path (reflection) and a reference path (transmission). Using a microscope objective, the signal path beam was strongly focused under normal incidence onto the substrate surface of a high-reflectivity mirror from its antireflection-coated side. For the beam's intensity profile, we determined a full Gaussian width of (5.29±0.06) µm, defining our setup's transversal resolution. The technique's resolution is fundamentally constrained only by diffraction.

The sample mirror consisted of a planar fused-silica substrate of 25.4-mm diameter and 6.35-mm thickness with a specified root-mean-square roughness of <0.8 nm. It had a high-reflection coating with a specified reflectivity of 99.95% for 1,550 nm applied by 3photon via ion beam sputtering. The back was antireflection coated. The technique is not constrained

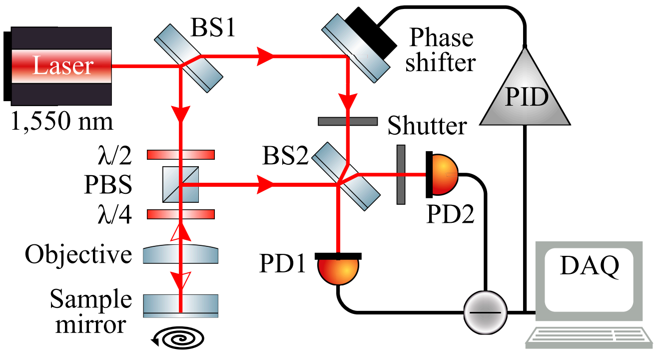

Fig. 1. Schematic of the experiment. BS1 and BS2 were balanced beam splitters forming a Mach–Zehnder interferometer. An objective lens focused the measurement beam through the sample substrate onto its surface beneath the reflection coating. The lens was corrected for the substrate thickness. The reflected beam was isolated using a combination of a polarizing beam splitter (PBS) and a quarter-wave plate. The interferometer was servo-controlled on half fringe. The phase was read out by recording the difference voltage of 2 photo diodes (PD) with a data acquisition card (DAQ). The 2 shutters were closed to measure the optical loss.

to highly reflective optics. Our objective was designed by ASE OPTICS to illuminate a sample through a 6.35-mm-thick fused silica coverplate. Utilizing this, we illuminated the sample mirror from the back to measure the substrate profile at the interface between substrate and high reflection coating. Therefore, the measurement was free from external impurities, such as dust particles adhering to the mirror, and provided information of the substrate's effective roughness. The setup is not limited to this configuration if a different objective design is used.

The sample mirror was attached to a combination of 2 motorized high-precision stages via a custom-made, ring-shaped mount that holds the substrate in place by friction as to not obstruct any of the optic. A rotation stage with vertical axis spun the centered mirror at a frequency of 5 Hz, while a linear stage moved the setup radially by 10 μm/s. Combined, they drove the sample mirror along a spiral scanning trajectory, mapping ring-shaped FOVs. To prevent gaps in the scan, the radial velocity needed to be smaller than one focus diameter per revolution. Simultaneously, the sampling rate must be sufficiently high to ensure that the sample spacing was always smaller than one beam diameter. The scanning duration then scales linearly with the radius of the FOV at fixed radial velocity and rotation frequency.

A mechanically stable periscope was built to enable normal incidence of the laser light. Alignment screws on the custom mirror mount were used to minimize the angular offset between the mirror's surface normal and the probe beam that would create beam pointing, reducing the interference contrast and quality of the focal plane. Upon precisely aligned retroreflection, the beam waist was put at the effective plane of reflection of the coating, i.e., close to the substrate surface underneath the coating. The focused probe beam acquired a microscopic reflection phase, depending on the height profile of the sample mirror's surface. The beam carrying this phase signal is isolated using a combination of a polarizing beam splitter and a quarter-wave plate. Two balanced photodiodes measured the interference result created by overlapping signal and reference paths at a second beam splitter (BS2), detecting the microscopic phase shift. While moving the stages, we measured an average fringe visibility of 96%. The differential voltage was recorded by a data acquisition card with 3.571 MSa/s and 16-bit resolution. Additionally, it was filtered by the proportional–integral–derivative controller and fed back to a mirror mounted to a piezo actuator (phase shifter), locking the interferometer to midfringe for optimal phase sensitivity [18]. The phase shifter consisted of a mirror mounted to a piezo actuator. We ramped the phase shifter to determine the slope at midfringe for calibration of photocurrent to reflection phase.

In the spectrum of large signal-to-noise ratios, the interferometer reached a noise floor of down to $(3.1\pm1.4)\ \mathrm{fm}/\sqrt{\mathrm{Hz}}$, which was close to the shot noise limit of $(2.5\pm1.2)\ \mathrm{fm}/\sqrt{\mathrm{Hz}}$. This can be seen in Fig. 2. Although the rotation frequency of the scan was just 5 Hz, strong signals appeared up to 60 kHz, as high frequency components corresponded to steep slopes in the measured phase profile. The steepest detectable slope was limited by convolution with the beam profile. Due to the spiral scanning, the probe beam had a large velocity relative to the sample mirror. Combined with the strongly focused spatial profile, this resulted in a very narrow temporal beam profile. Consequently, the beam had a broad spectral profile, enveloping the reflection phase spectrum. Since the relative beam velocity depended on the radius and continuously changes during the scan, the final spectrum was not Gaussian but the integral over a family of Gaussian profiles of increasing width.

Alternatively to the reflection phase, the almost identical setup was used to measure the spatially resolved optical loss of the laser mode. With the reference beam and one photodiode blocked, we recorded an optical loss map of the same FOV, resolution, and topology as the phase map, providing information of surface scattering and absorption. By splitting the reflected light beam for 2 complementary observations, future implementations could even measure 2 observables simultaneously.

Data processing

We used a spectral filter to suppress interference caused by acoustic vibrations and imperfections in the motorized stages. All frequency components below 2.5 kHz for the phase measurements and below 0.5 kHz for the loss measurements were removed. To reduce the calculation time, we processed all recorded data in subsets corresponding to one revolution. Filtering proved to be very effective in removing noise and

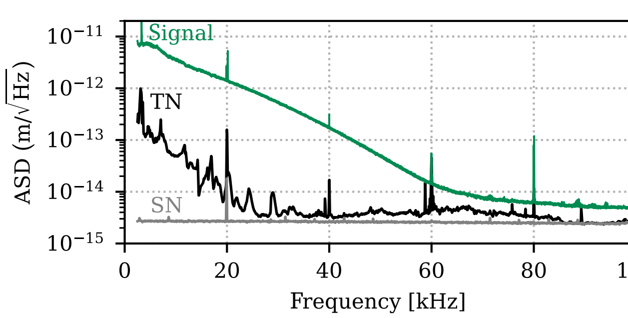

Fig. 2. Measurement data. Amplitude spectral density (ASD) of the interferometer signal when scanning the surface at 5 Hz within the radii of 3.5 to 5.5 mm. "TN" is the total noise measured while the sample position was stationary, and "SN" is the shot noise measured with a blocked signal path and then multiplied by $\sqrt{2}$. All traces were averaged 1,000 times. TN and SN have a resolution bandwidth of 53 Hz and the signal spectrum 5 Hz. Below 60 kHz, the average signal-to-noise ratio calculates to 32 dB.

minimizing artifacts that inevitably occurred on steep signal slopes and at the edges of datasets.

Phase maps and loss maps were reconstructed in the following way. We spiraled the entire dataset and initially assumed that both the rotation stage and the linear stage were working uniformly. We were able to correct for deviations from the constant rotation frequency and the constant displacement speed, as the data partially overlapped spatially and showed local occurrences. As our data acquisition led to oversampling, we then summarized all the measured values of a surface with an edge length of 2 μm into a single pixel value. Two micrometers corresponded to the radial distance, and the focused laser spot moved over the course of one rotation. The pixel's value was set to the arithmetic mean.

The reflection phase value of each pixel was converted into a distance change for the propagating laser light. The reconstructed map thus showed a height profile of the interface between the substrate surface and the dielectric high-reflection coating. This resulted in a lower limit for the surface roughness of the substrate. It was a lower limit because both the first dielectric layers of the mirror coating and the size of the beam waist of our laser beam slightly smoothen the surface roughness. We therefore use the term effective roughness. To determine the loss map, it was assumed that the amount of reflected light from areas without explicit, localized loss corresponds to a perfect reflection. For this purpose, the mean value of all pixels minus those with explicit absorption was set to 100% reflection. We then defined the deviation from this mean value as the relative optical loss.

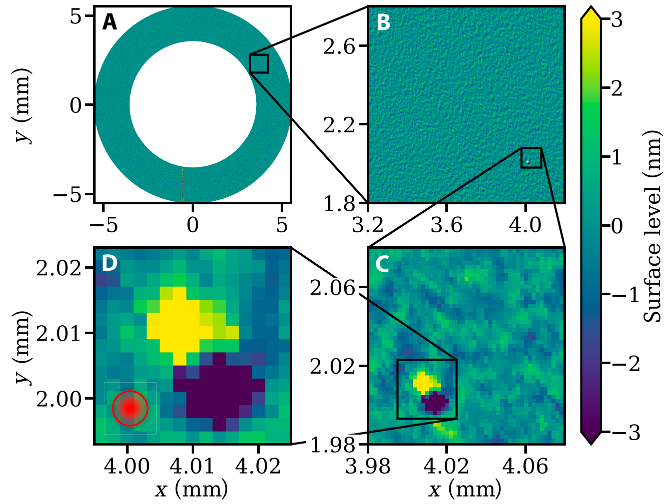

Fig. 3. Reconstructed map of measured reflection phase. Reflection phase was measured per beam area ≈22 μm^2 and is expressed in terms of surface level with a conversion factor of 11.71 mrad/nm. (A) Overview of a full spiral scan of 2-mm radial width. (B) Section of (A), enlarged by a factor of 10, showing the effective roughness profile of the sample mirror substrate. (C) Section of (B), enlarged by a factor of 10, showing a microscopic phase feature. (D) Section of (C), enlarged by a factor of 3, comparing the feature to the focus diameter, indicated by a black, Gaussian intensity distribution and a circle corresponding to its waist. Transversal resolution was 5.29 μm.

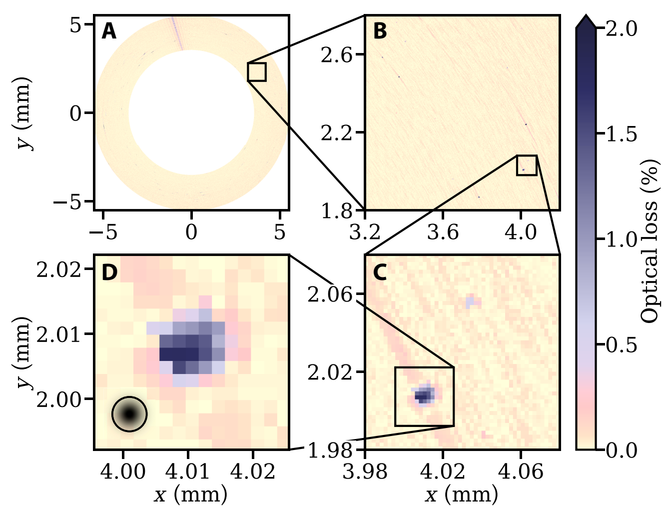

Fig. 4. Reconstructed map of measured optical loss. Optical loss was measured per beam area ≈22 μm^2. The corresponding transversal resolution was 5.29 μm^2. (A) Overview of full scan. (B) Section of (A), enlarged by a factor of 10, showing the same spatial excerpt as Fig. 3B. (C) Section of (B), enlarged by a factor of 10, showing a microscopic spot of high optical loss. (D) Section of (C), enlarged by a factor of 3, comparing the feature to the probe beam's focus diameter. Feature areal density is roughly 12 features per square millimeter.

Results

Interferometric phase map of substrate to coating interface

Figure 3 shows a reconstructed reflection phase profile map scanned from 3.5- to 5.5-mm radius, at the time limited by a slight misalignment of the linear stage. It nevertheless covers an area of about 56 mm^2, corresponding to more than 11% of the sample mirror's surface area. The measurement took about 3 min and the postprocessing another 3 min. The map shown was reproducible even after realigning the setup days apart.

Figure 3A provides an overview of the scanned area. It shows an edge artifact at the bottom in the form of a line, which originates from the circulating data processing. Figure 3B shows an enlarged excerpt of Fig. 3A where the surface profile becomes visible. It is a random but coherent profile spanning the entire FOV. We find an effective roughness of (590±24) pm, agreeing with the manufacturer's specification of <800 pm. We note that an even stronger agreement of these 2 values is not expected as the presented method averages over the laser beam's waist area of about 22 μm.

We additionally observe localized features of large phase amplitude, which are sparsely scattered over the sample, as shown in Fig. 3C and D. All features show an oscillation between a negative and positive surface level. This behavior possibly originates from the spectral filtering, as it shows a correlation to the filter's threshold frequency and only appears along the angular axis.

Optical loss map of substrate to coating interface

Figure 4 shows the optical loss map for the same surface as in Fig. 3. The overview (Fig. 4A) reveals that most of the FOV is "empty", showing a very weak background and emphasizing the mirror's quality. The top line again originates from edge artifacts. In Fig. 4B, there are also some slight artifacts in angular direction at the sensitivity limit of the measurement. We again observe sparsely scattered microscopic features, as shown in Fig. 4C and D. They cause up to 62% of optical loss per beam area of about 22 μm^2. All point absorbers taken together reduced the average reflectivity of the surface by only 0.01%. This value is significantly smaller than the maximum deviation from perfect mirror reflectivity specified by the manufacturer ($R \geq 99.95\%$).

Correlations between loss and phase maps

We find that many features appear in both maps at the same position; see Fig. 5A to C. Some features, however, only appear strongly in one map. Consequently, the observed features must fall into different categories. The differences in the maps were reproducible in repeated measurements after renewed alignment optimization.

Features appearing predominantly in the effective roughness map are required to produce a phase shift, while not causing any substantial optical loss by scattering, absorption, or transmission. This would be the case for local steps in the atomic surface profile. If features appear equally strong in both maps, additionally, they are required to cause some optical loss for example due to optically scattering defects. Finally, peaks predominantly visible in the optical loss map must not experience any considerable phase shift. We consider it likely that absorption was the dominating loss effect, as we measured optical loss of up to 62%. Due to the high numerical aperture of our microscope objective and the highly reflective coating behind the feature, neither scattered nor transmitted light would have resulted in any major loss.

Even though our laser spot intensity ($\approx 2.3 \times 10^7$ W/m^2) was very much comparable to the intensity in Advanced LIGO ($\approx 1.7 \cdot 10^7$ W/m^2)[5,19], we did not expect thermal effects to influence the phase signal over extended areas, as our laser spot moved rapidly over the optic rather than continuously illuminating it. We expected heat to dissipate into the substrate volume faster than the laser spot required for one rotation.

Conclusion

We present tomographic laser scanning microscopy for profiling optical surfaces regarding phase and loss topography. We demonstrate its potential in an experimental setup, yielding partly correlated phase and optical loss maps of the same FOV and topology. These images cover an area of 56 mm^2, while having 5-μm resolution and close to shot-noise limited phase sensitivity corresponding to about 3 fm/$\sqrt{\text{Hz}}$. A full-size high-resolution map required a measurement time of around 3 min plus the computing time of a standard PC of a further 3 min.

On our sample mirror, we observe a cohesive but random reflection phase profile corresponding to an effective roughness of the substrate surface. In both the phase map and the optical loss map, we find point-like features. Our technique allows for correlations between phase and loss topography to be revealed, which should provide a better understanding of limiting imperfections in optical surfaces. Such include point absorbers, which are a current problem for high-laser-power applications, like gravitational wave detectors [10,11].

Due to the spiral scanning approach, the measurement duration is short and scales with the FOV's radius instead of its area. There is no conceptual limit to the FOV size, and using optimized algorithms, real-time data processing in parallel to the measurement is realistic. This makes the presented method a viable option even for large optics like those used in gravitational wave detectors or industrial wafers, without compromising resolution.

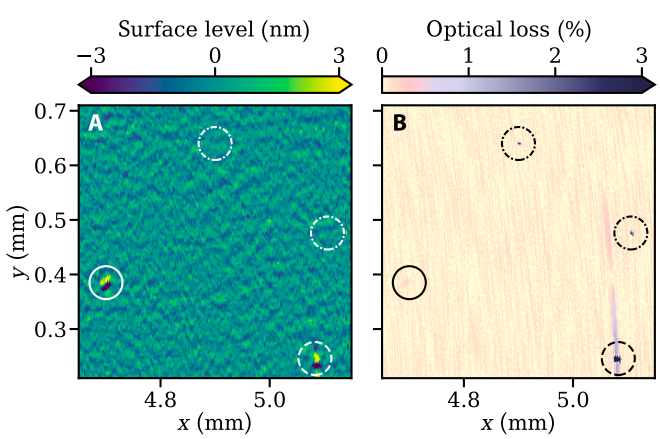

Fig. 5. Correlations between loss and phase maps. (A) Section of the effective roughness profile. (B) Same section as in (A), showing the optical loss. The solid circle contains a feature strongly visible only in the phase map, possibly a local step in the atomic surface profile or the refractive index. The dashed circle contains a feature strongly visible in both maps with an optical loss of 30%. The dash-dotted circles highlight features appearing only in the loss map. We consider it likely that all 3 features are point absorbers. The background pattern in (A) also corresponds to the actual surface profile of the substrate. The 2 lower highlighted features show color artifacts due to the steep phase profile and filtering during postprocessing of the data. The background pattern in (B) is entirely due to filtering artifacts.

Acknowledgments

Funding: This work was funded by the Deutsche Forschungsgemeinschaft (DFG, German Research Foundation) under Germany's Excellence Strategy EXC 2121 "Quantum Universe" 390833306.
Author contributions: L.A. conducted the experiment. M.H. prepared the experiment and helped in conducting the experiment. R.S. conceived the idea and designed the experiment. All authors wrote the paper.
Competing interests: The authors declare that there is no conflict of interest related to this article.

Data Availability

Data underlying the results presented in this paper are not publicly available at this time but may be obtained from the authors upon reasonable request.

References

1. Schreiber KU, Klügel T, Wells J-PR, Hurst RB, Gebauer A. How to detect the Chandler and the annual wobble of the Earth with a large ring laser gyroscope. *Phys Rev Lett*. 2011;107(17):Article 173904.
2. Skeldon KD, Mackintosh J, von Gradowski M, Thieux S, Lee R. Qualification of supermirrors for ring-laser-gyros based on surface roughness and scatter measurements. *J Opt A Pure Appl Opt*. 2001;3:183.
3. Ludlow A, Boyd MM, Ye J, Peik E, Schmidt PO. Optical atomic clocks. *Rev Mod Phys*. 2015;87:637.
4. Kessler T, Hagemann C, Grebing C, Legero T, Sterr U, Riehle F, Martin MJ, Chen L, Ye J. A sub-40-mHz-linewidth laser based on a silicon single-crystal optical cavity. *Nat Photonics*. 2012;6:687–692.
5. LIGO Scientific Collaboration, Aasi J, Abbott BP, Abbott R, Abbott T, Abernathy MR, Ackley K, Adams C, Adams T,

Addesso P, et al. Advanced LIGO. *Class Quantum Gravity*. 2015;32(7):Article 074001.
6. The VIRGO Collaboration, Beauville F, Buskulic D, Flaminio R, Marion F, Masserot A, Massonnet L, Mours B, Moreau F, Ramonet J, et al. The VIRGO large mirrors: A challenge for low loss coatings. *Class Quantum Gravity*. 2004;21(5):S935.
7. Sato S, Miyoki S, Ohashi M, Fujimoto MK, Yamazaki T, Fukushima M, Ueda A, Ueda KI, Watanabe K, Nakamura K, et al. Loss factors of mirrors for a gravitational wave antenna. *Appl Opt*. 1999;38(13):2880–2885.
8. Elson JM, Rahn JP, Bennett JM. Light scattering from multilayer optics: Comparison of theory and experiment. *Appl Opt*. 1980;19(5):669–679.
9. Vahlbruch H, Chelkowski S, Danzmann K, Schnabel R. Quantum engineering of squeezed states for quantum communication and metrology. *New J Phys*. 2007;9:371.
10. Jia W, Yamamoto H, Kuns K, Effler A, Evans M, Fritschel P, Abbott R, Adams C, Adhikari RX, Ananyeva A, et al. Point absorber limits to future gravitational-wave detectors. *Phys Rev Lett*. 2021;127(24):Article 241102.
11. Brooks AF, Vajente G, Yamamoto H, Abbott R, Adams C, Adhikari RX, Ananyeva A, Appert S, Arai K, Areeda JS, et al. Point absorbers in Advanced LIGO. *Appl Opt*. 2021;60(13):4047–4063.
12. Chkhalo N, Churin S, Pestov A, Salashchenko NN, Vainer YA, Zorina MV. Roughness measurement and ion-beam polishing of super-smooth optical surfaces of fused quartz and optical ceramics. *Opt Express*. 2014;22(17): 20094–20106.
13. Gong Y, Xu J, Buchanan RC. Surface roughness: A review of its measurement at micro-/nano-scale. *Phys Sci Rev*. 2018;3(1):20170057.
14. Eaton P, West P. *Atomic force microscopy*. Oxford (UK): Oxford Univ. Press; 2010.
15. De Groot P. Coherence scanning interferometry. In: Leach R, editor. *Optical measurement of surface topography*. Berlin, Heidelberg (Germany): Springer; 2011. p. 187–208.
16. De Groot P. Principles of interference microscopy for the measurement of surface topography. *Adv Opt Photon*. 2015;7(1):1–65.
17. Wyant JC. *Holography: A tribute to Yuri Denisyuk and Emmett Leith*. Bellingham (WA): SPIE; 2002. vol. 4737, p. 98–107.
18. Dowling JP, Seshadreesan KP. Quantum optical technologies for metrology, sensing, and imaging. *J Lightwave Technol*. 2014;33(12):2359–2370.
19. Yu H, McCuller L, Tse M, Kijbunchoo N, Barsotti L, Mavalvala N, members of the LIGO Scientific Collaboration. Quantum correlations between light and the kilogram-mass mirrors of LIGO. *Nature*. 2020;583:43–47.